Formation of Vacancies in Si- and Ge-based Clathrates: Role of Electron Localization and Symmetry Breaking

Amrita Bhattacharya,[1] Christian Carbogno,[1] Bodo Böhme,[2] Michael Baitinger,[2] Yuri Grin,[2] and Matthias Scheffler[1,3,4]
[1]*Fritz Haber Institute of the Max Planck Society, Faradayweg 4-6, 14195 Berlin, Germany*
[2]*Max-Planck-Institut für Chemische Physik fester Stoffe, Nöthnitzer Str. 40, 01187 Dresden, Germany*
[3]*Department of Chemistry and Biochemistry, University of California at Santa Barbara, Santa Barbara, California 93106, USA*
[4]*Materials Department, University of California at Santa Barbara, Santa Barbara, California 93106, USA*
(Received 3 March 2016; revised manuscript received 25 October 2016; published 6 June 2017)

The formation of framework vacancies in Si- and Ge-based type-I clathrates is studied using density-functional theory as a function of filling the cages with K and Ba atoms. Our analysis reveals the relevance of structural disorder, geometric relaxation, and electronic saturation as well as vibrational and configurational entropy. In the Si clathrates, we find that vacancies are unstable, but very differently, in Ge clathrates, up to three vacancies per unit cell can be stabilized. This contrasting behavior is largely driven by the different energy gain on populating the electronic vacancy states, which originates from the different degree of localization of the valence orbitals of Si and Ge. This also actuates a qualitatively different atomic relaxation of the framework.

DOI: 10.1103/PhysRevLett.118.236401

Clathrates are compounds with complex and large cage-like crystal structures (*hosts*) that can be filled with *guest* atoms or molecules (Fig. 1) [1]. Charge and heat transport in intermetallic clathrates have been studied intensively over the last decade [2] since filling would allow us to increase their thermoelectric efficiency [3]. The uttermost majority of filled clathrates are, however, metallic [4–9] and thus, unsuitable for this application in their pristine form. Nonetheless, puzzling exceptions exist, e.g., Ge_{46} filled with K: after decades of experiments [4–6], its semiconducting character was recently explained by a careful structure analysis [10], which revealed a high vacancy concentration (∼4%). For this case, the puzzle appears to be resolved [11,12]. However, high-quality synthesis and experimental analysis have remained challenging in this field. In particular, no fundamental understanding exists of the mechanism that determines vacancy formation and thus composition, structure, and electronic character upon filling. Therefore, these properties of clathrates are still unpredictable in practice.

The most prominent example is the isoelectronic Si and Ge type-I clathrates (see Fig. 1): these clathrates exhibit comparable properties in the unfilled case (cf. Table I and Ref. [13]) but behave remarkably different upon filling, e.g., with K or Ba guests. In the case of Si, the framework remains intact, and metallic behavior (e.g., K_8Si_{46} [4–6] and Ba_8Si_{46} [7–9]) results. In the case of Ge, vacancies □ occur in the host framework: in line with Zintl's concept, a heavily doped semiconductor $K_8Ge_{44}□_2$, featuring two framework vacancies, was found experimentally for monovalent K guests [6,10]. For divalent Ba fillers, however, experiments [14,15] found a metallic $Ba_8Ge_{43}□_3$ compound with three vacancies, but not four, as expected from the increased Ba valence. In this Letter, we present a quantitatively reliable theoretical prediction of the structure, composition (vacancy concentration), electronic structure, and thermodynamic stability for the binary K/Ba-Si/Ge systems. These findings explain the existing experimental results and provide an atomistic mechanism for the contrasting behavior of Si and Ge clathrates.

Density-functional theory (DFT) [16,17] calculations were performed with FHI-aims [18,19], an all-electron, full-potential electronic-structure code that uses numeric atom-centered basis sets. Numerical settings were chosen to achieve a convergence in energy differences better than 10^{-3} eV/atom (see Supplemental Material [20]). To ensure that our findings are independent from the chosen treatment

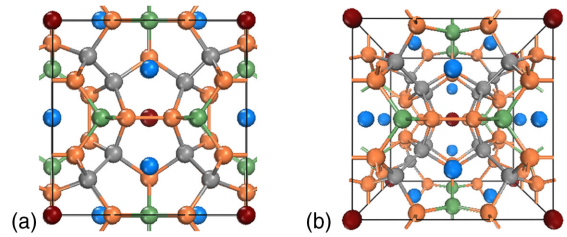

FIG. 1. The (a) normal and (b) orthographic projection (along [100]) of the crystal structure (space group $Pm\bar{3}n$) of type-I clathrates [2]. Colors denote the Wyckoff sites for the host (6*c*-green, 16*i*-grey, and 24*k*-orange) and the guest atoms (2*a*-red, 6*d*-blue).

TABLE I. Properties of empty Si_{46} and Ge_{46} clathrates computed in the 46-atom unit cell for various xc functionals: lattice parameter a_0 (Å), cohesive energy E_c (eV), Kohn-Sham band gap ϵ_g (eV), neutral vacancy formation energy $E^0_\square$ (eV), and charge transition level $I_{0/4-}$ with respect to the top of the valence band. The atomic chemical potential (for E_c and $E^0_\square$) is that of the diamond type structure.

	Si_{46}					Ge_{46}				
	a_0	E_c	ϵ_g	$E^0_\square$	$I_{0/4-}$	a_0	E_c	ϵ_g	$E^0_\square$	$I_{0/4-}$
LDA	10.11	3.8	1.14	3.33	0.93	10.49	2.2	1.25	2.97	0.60
PBEsol	10.17	3.4	1.21	3.35	0.95	10.59	1.9	1.23	2.92	0.58
PBE	10.23	2.7	1.33	3.43	1.10	10.74	1.5	1.12	2.80	0.57
RPBE	10.30	2.0	1.43	3.50	1.08	10.84	1.0	1.09	2.77	0.58
HSE06	10.18	3.4	1.90	3.85	1.48	10.62	1.7	1.89	3.32	0.95

for exchange and correlation (xc), we compare how various xc functionals describe both the equilibrium properties of the empty F_{46} clathrates (F = Si, Ge) and the charged vacancy [21]. Its formation energy is calculated using the total energy difference

$$E^q_\square = E(F_{45}\square^q_1) - E(F_{46}) + \frac{E(F^{\mathrm{Dia}}_2)}{2} + q(\mu_e - \mathrm{VBM}) \quad (1)$$

between the defective framework $E(F_{45}\square^q_1)$ with charge q and the pristine clathrate $E(F_{46})$ [22]. The diamond phase $E(F^{\mathrm{Dia}}_2)$ and the electron chemical potential μ_e relative to the valence band maximum VBM act as thermodynamic reservoirs. The VBM of the defective and of the pristine clathrate ($\mathrm{VBM}^{\mathrm{Pr}}$) are referenced using the core level shift ΔV between $F_{45}\square^q_1$ and F_{46}: $\mathrm{VBM} = \mathrm{VBM}^{\mathrm{Pr}} + \Delta V$. Charge transition levels $I_{q/q'}$, which quantify the energy involved in charging the vacancy [22], are computed using the value of μ_e at which $F_{45}\square^{q'}_1$ and $F_{45}\square^q_1$ are in equilibrium

$$I_{q/q'} = \frac{E(F_{45}\square^{q'}_1) - E(F_{45}\square^q_1)}{q - q'} + \mathrm{VBM}. \quad (2)$$

For the local-density approximation (LDA) [23]), variants of the generalized gradient approximation (Perdew-Burke-Ernzerhof exchange-correlation functional PBE [24], as well as the adaption of PBE for solids PBEsol [25], and the revised PBE parameterization RPBE [26]) and the computationally more expensive Heyd-Scuseria-Ernzerhof functional (HSE06 [27]) that incorporates a fraction of exact exchange, Table I lists the lattice parameter a_0, cohesive energy E_c, and band gap ϵ_g for the empty F_{46} clathrates as well as the formation energy for a neutral vacancy $E^0_\square$ at the 6c site and its transition level $I_{0/4-}$, which characterizes the typical charge state in these clathrates (see below). We find the typical over/underbinding of LDA/PBE for a_0 and E_c, whereby PBEsol gives results similar to HSE06 (differences are $< 0.5\%$ for a_0 and < 5 meV/atom for E_c). Deviations in the vacancy formation energies $E^0_\square$ and transition levels $I_{0/4-}$ are, however, noticeable. In the following, PBEsol was thus employed in the structural search. We explicitly checked that the relative energetic ordering of the thereby identified compositions is retained with HSE06 (see Supplemental Material [20]).

To determine the stable vacancy concentrations in Si and Ge frameworks filled with K or Ba guests (G), we have first identified the energetically favorable configurations for all compositions $G_nF_{46-y}\square_y$, with $n \in [0, 8]$ guests and $y \in [0, 4]$ vacancies, using an iterative strategy that required ~1400 full structural relaxations: starting from the completely filled clathrate, we have first identified the most favorable vacancy sites by scanning over all possible framework positions. Then, we stepwise removed guests from the compositions with fully occupied and defective framework, again scanning over all available guest sites. For any subsequent composition, we retained the already identified guest and vacancy sites and thus, limited the scanning to the remaining available positions. Eventually, we computed the formation energies of these compositions using the stochiometrically balanced energy difference

$$E_f(n, y) = E(G_nF_{46-y}\square_y) - \frac{46 - y - n \cdot x}{2} \cdot E(F^{\mathrm{Dia}}_2) - n \cdot E(G_1F_x) \quad (3)$$

between the filled and/or defective clathrate $E(G_nF_{46-y}\square_y)$ and the reservoirs for framework F and guest atoms G, i.e., F^{Dia}_2 and the thermodynamically stable neighboring phases G_1F_x (K_4Si_4 [28], $BaSi_2$ [29], K_4Ge_4 [30], and Ba_6Ge_{25} [31]). As the formation energy differences in Fig. 2 show, vacancy formation is always energetically unfavorable in Si clathrates by $\Delta E_f > 0.3$ eV/vacancy but not in Ge clathrates: in the fully filled case, divacant $K_8Ge_{44}\square_2$ and trivacant $Ba_8Ge_{43}\square_3$ are energetically favorable by $\Delta E_f < -0.1$ eV/vacancy; partial filling ($n < 8$) makes smaller vacancy concentrations preferable [32].

Figure 2 also reveals that vacancy formation energies generally decrease with increasing filling so that the

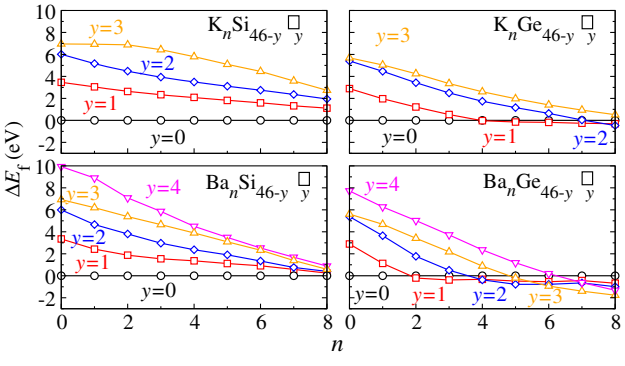

FIG. 2. Calculated (DFT PBEsol) formation-energy difference $\Delta E_f = E_f(G_nF_{46-y}\square_y) - E_f(G_nF_{46})$ as a function of the filling n, with K and Ba guests.

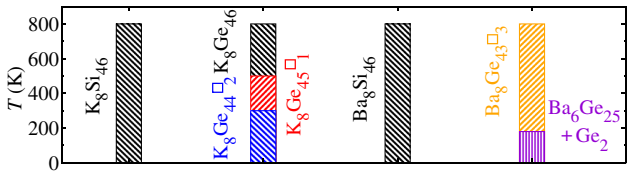

FIG. 3. Most favorable compositions of K/Ba-filled Si/Ge clathrates as a function of temperature T computed at the DFT PBEsol level.

question arises: if the fully filled clathrates identified as stable at 0 K are also the most stable ones at finite temperatures. To clarify, their thermodynamic stability was computed by accounting for configuration entropy and vibrational free energies (see Supplemental Material [20]). As shown in Fig. 3, the compositions discussed above (K_8Si_{46}, $K_8Ge_{44}\square_2$, Ba_8Si_{46}, $Ba_8Ge_{43}\square_3$) are also stable at room temperature. Interestingly, vacancies in the K-filled Ge clathrate become less favorable with increasing temperature, which reflects that their formation is energetically favorable but entropically adverse due to the harder vibrations present in defective frameworks (see Supplemental Material [20]). Since this compound is typically synthesized at temperatures > 600 K [4–6,10], this explains reports of less than two vacancies per unit cell [33]. Accordingly, calculations correctly reproduce the trends in formation and phase stability for all compositions observed experimentally [5,7,10], including the eutectoid decomposition of $Ba_8Ge_{43}\square_3$ [15].

Furthermore, calculations consistently reproduce the electronic character found for these compositions experimentally: the guests donate electrons to the framework, which leads to a partial filling of the conduction band and thus, to a metallic electronic structure in the stable vacancy-free Si clathrates (8 and 16 charge carriers/f.u. for K and Ba with $n = 8$). Conversely, the vacancies in the Ge framework accommodate up to four surplus electrons each, as suggested by qualitative models [11,12]. Because of the completely occupied vacancy states, $K_8Ge_{44}\square_2$ is a semiconductor with a band gap of 0.18/0.28 eV (PBEsol/HSE06). Similarly, all vacancy states are occupied in $Ba_8Ge_{43}\square_3$, but the four additional electrons accommodated in the conduction band lead to a metallic electronic structure.

Our studies confirm that filled Si- and Ge-based clathrates behave remarkably, even qualitatively, differently in spite of their isoelectronicity. Figure 2 also suggests the mechanism that stabilizes vacancies in Ge but not in Si: in Ge, the slope $\partial\Delta E_f(n,y)/\partial n$ changes significantly whenever the number of guest atoms n matches $n = 4y/z$ (z is the valency of the guest cation), e.g., for $K_4Ge_{45}\square_1$ or $Ba_4Ge_{44}\square_2$. Regardless of the guests' species, the Ge compositions meeting this condition are energetically favorable and are the only ones that exhibit semiconducting character. Conversely, such distinct changes in the slope are not observed in Si, for which $\partial\Delta E_f(n,y)/\partial n$ is almost independent on the number of guests. Since $\Delta E_f(n,y)$ is defined as the energy difference between the defective and the completely occupied host framework, its slope $\partial\Delta E_f(n,y)/\partial n$ is related to the energy gain stemming from charging the vacancy.

In more detail, this mechanism can be rationalized by inspecting the electronic structure of these defected clathrates: as sketched in Fig. 4, the guests lose their valence electrons in state ϵ_G to the energetically lower-lying conduction band minimum ϵ_{CBm} or—if available—to the vacancy states $I_{q/q'}$ in the band gap. The respective energy gains are $E_{CBm} = \epsilon_G - \epsilon_{CBm}$ and $E_{q/q'} = \epsilon_G - I_{q/q'}$. In first-order approximation, their difference $\Delta E_{q/q'} = E_{CBm} - E_{q/q'}$ determines the slope $\partial\Delta E_f(n,y)/\partial n$ for $n \le 4y/z$. Please note that by definition, $\Delta E_{q/q'}$ is not particularly sensitive on the guests' species (see Supplemental Material [20]) but is predominantly determined by the host. Surprisingly, this reveals that the contrasting tendency to suppress or form vacancies in Si and Ge frameworks is largely controlled by the charge transition levels of their vacancies. Indeed, Figs. 2 and 4 consistently show that both $\partial\Delta E_f(n,y)/\partial n$ and $\Delta E_{q/q'}$ are much smaller in Si than in Ge. Accordingly, the different properties of a single vacancy in guest-free $Si_{45}\square_1$ and $Ge_{45}\square_1$ also allow us to rationalize the underlying mechanism: quantitatively, the energetic cost $E^0_\square$ to create a neutral vacancy is indeed slightly higher by $\approx$0.4 eV in Si (cf. Table I); the energetic gain $\Delta E_{0/4-} = -4(\epsilon_{CBm} - I_{0/4-})$ obtained from fully charging the vacancy is, however, distinctly larger in Ge by ≈ -1.2 eV and thus, exceeds the cost of creating a vacancy—but only if geometric relaxations are accounted for (cf. Fig. 4). In the unrelaxed case, the charge transition levels $I_{q/q'}$ show only slight quantitative differences for Si and Ge but the exact same qualitative behavior. Upon structure relaxation, however, the charge transition levels in Si form energetically almost degenerate, zero-U [34] pairs $I_{0/1-}$ and $I_{1-/2-}$ as well as $I_{2-/3-}$ and $I_{3-/4-}$, whereby $I_{0/4-}$ is virtually unaltered. Conversely, the individual levels, including $I_{0/4-}$, undergo

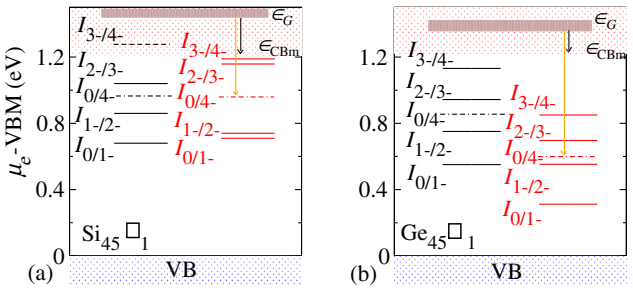

FIG. 4. Calculated (DFT PBEsol) charge transition levels $I_{q/q'}$ of (a) $Si_{45}\square_1$ and (b) $Ge_{45}\square_1$ with the unrelaxed (black) and fully relaxed (red) structure. Schematically, the positions of the guest levels ϵ_G in the conduction band are drawn to highlight the energy gains E_{CBm} and $E_\square$ associated with electron transfer from ϵ_G to the conduction band minimum ϵ_{CBm} (black arrow) and to the vacancy's ionization level $I_{0/4-}$ (orange arrow).

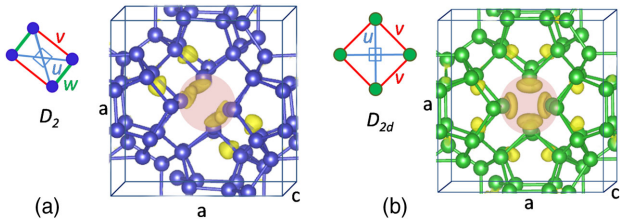

FIG. 5. Symmetry of the calculated (DFT PBEsol) atomic arrangements around the relaxed $F_{45}\square_1^{4-}$ vacancy in empty (a) Si and (b) Ge clathrates. The isosurface (isovalue 0.015 eÅ^{-3}) of the charge density difference with respect to the uncharged system $F_{45}\square_1^0$ is shown; the vacancy region is highlighted.

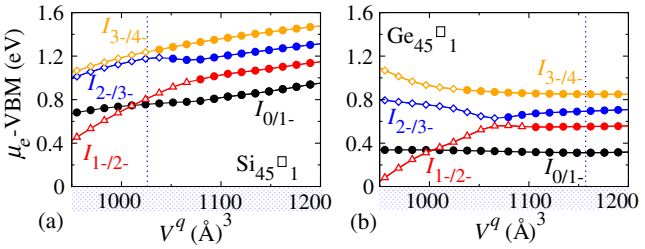

FIG. 6. Calculated (DFT PBEsol) charge transition levels $I_{q/q'}$ of (a) $Si_{45}\square_1$ and (b) $Ge_{45}\square_1$ as a function of unit cell volume V^q, with vacancies in charge state q (filled circle corresponds to a D_{2d} symmetry, diamond to D_2, and triangle denotes the situation when q and q' differ in symmetry). The vertical lines denote the scenarios at the equilibrium volume.

distinct shifts to lower energies in Ge, which explains the large overall energy gain $\Delta E_{q/q'}$. This demonstrates that the contrasting behavior of Si and Ge clathrates is neither driven by guest-host interactions nor by the different cost of creating neutral vacancies but is predominantly determined by electron transfer processes upon charging.

These electron transfer processes result from the different character of the Si and Ge transition levels, which arise from different geometric distortions. Qualitatively, this is reflected in the electron distribution around the vacancy (Fig. 5). Quantitatively, we use the interatomic distances u, v, and w between the vacancies' neighbors (cf. Fig. 5 and [35,36]) and the lattice parameter ratio c/a to characterize the local and global symmetry. In the unrelaxed case ($c/a = 1$), the neutral vacancy exhibits a global D_{2d} symmetry with nearest-neighbor distances u (3.90 Å in Si, 4.07 Å in Ge) and $v = w$ (3.86 Å in Si, 4.02 Å in Ge). In the case of $Ge_{45}\square_1$, the local D_{2d} symmetry ($u = 3.15$ Å, $v = w = 3.39$ Å) and the cubic lattice ($c/a \leq 1.01$) are essentially retained when relaxing the fully charged vacancy. Conversely, we find that the fully charged Si vacancy features a local D_2 symmetry ($u = 2.98$ Å, $v = 3.55$ Å), with a drastically shortened pair of distances $w = 3.07$ Å. Also, a *global* break in lattice symmetry (tilting $\gamma = 92°$ and $c/a = 1.02$) occurs, which results in a splitting of the charge density around the vacancy in two distinct lobes. The same qualitative behavior also occurs in filled clathrates (see Supplemental Material [20]). Please note that contrasting local relaxation patterns have been reported for the vacancy in the respective Si and Ge diamond phases [35,36], too, but not a global symmetry break as in this case.

This peculiar and contrasting relaxation behavior of vacancies in clathrates can be attributed to the fact that the $3sp^3$ valence orbitals in Si_{46} are spatially more localized than the $4sp^3$ orbitals in Ge_{46}. Accordingly, the Si framework is more rigid, which results in almost twice as high phonon frequencies (see Supplemental Material [20]). In turn, this allows local atomic and global lattice degrees of freedom to decouple and to break the symmetry independently. Thus, vacancy creation in empty Si_{46} leads to pairs of energetically unfavorable spatially localized noninteracting states ($I_{0/1-} \approx I_{1-/2-}$ and $I_{2-/3-} \approx I_{3-/4-}$, Fig. 4). Conversely, the charged vacancy in $Ge_{45}\square_1$ forms a bulk state that retains the global symmetry and spans the vacancy in spite of the large nearest-neighbor distances. Simultaneously, this lowers the charge transition levels upon relaxation. This interpretation in terms of localization of valence orbitals is substantiated by the volume dependence of the charge transition levels shown in Fig. 6. For all charge states q, we have computed $E_\square^q$ at different volumes in both the lattice configurations, with a local D_2 and D_{2d} symmetry, i.e., for the different c/a ratios and tiltings γ discussed before and listed in the Supplemental Material [20]. The energetically most favorable $E_\square^q$ is used to determine the transition levels $I_{q/q'}$. Expanding $Si_{45}\square_1$ and thus, enforcing an increased delocalization results in D_{2d}-type charge transition levels. Conversely, lattice compression (enforced localization) leads to D_2-type levels in $Ge_{45}\square_1$ (Fig. 6). This shows that the discussed effects, which are driven by global and local symmetry breaking, are inherently related to the relationship between nearest-neighbor distance (more than ~10% larger in clathrates than in the respective diamond structures) and valence orbital localization.

In summary, this Letter shows that vacancy formation is energetically not favorable for Si clathrates of K and Ba. Conversely, two vacancies per unit cell are formed in Ge clathrates fully filled with K and three vacancies in the case of Ba. In turn, this determines the different electronic character of these compounds. Regardless of the guest, the decisive energetic contribution for this contrasting behavior does not stem from the guests-host interaction or the formation of the neutral vacancy but from its charging. The occurring electron transfer processes are quantitatively and qualitatively different in Si and Ge since their different degree of valence orbital localization leads to contrasting structural relaxation patterns (global and local symmetry breaking). The stoichiometry, thermodynamic stability, and electronic structure of these materials is thus determined by the microscopic mechanism, which arises from the large ratio of nearest-neighbor distance and valence orbital localization. Accordingly, our study suggests that this mechanism can be influential also in other materials with

elongated bonds, e.g., skutterudites [37], Heusler alloys [38], boroncarbides [39], and perovskites [40]. Also in these cases, vacancy formation and its influence on structural and electronic properties are lively topics of research [41–44].

The data as well as the input and output files are available through NOMAD [45].

The authors thank Sergey Levchenko and Patrick Rinke for many fruitful discussions. The project received funding from the Einstein foundation (project ETERNAL), and the European Union's Horizon 2020 research and innovation program under Grant agreement No. 676580 with The Novel Materials Discovery (NOMAD) Laboratory, a European Center of Excellence.

[1] T. Takabatake, K. Suekuni, T. Nakayama, and E. Kaneshita, Rev. Mod. Phys. **86**, 669 (2014).
[2] *The Physics and Chemistry of Inorganic Clathrates* edited by G. S. Nolas (Springer, Dordrecht, 2014).
[3] M. Christensen, S. Johnsen, and B. B. Iversen, Dalton Trans. **39**, 978 (2010).
[4] C. Cros, M. Pouchard, and P. Hagenmuller, J. Solid State Chem. **2**, 570 (1970).
[5] G. K. Ramachandran and P. F. McMillan, J. Solid State Chem. **154**, 626 (2000).
[6] H. G. von Schnering, J. Llanos, K. Peters, M. Baitinger, Y. Grin, and R. Nesper, Z. Kristallogr. New Cryst. Struct. **226**, 9 (2011).
[7] S. Yamanaka, E. Enishi, H. Fukuoka, and M. Yasukawa, Inorg. Chem. **39**, 56 (2000).
[8] R. Lortz, R. Viennois, A. Petrovic, Y. Wang, P. Toulemonde, C. Meingast, M. M. Koza, H. Mutka, A. Bossak, and A. San Miguel, Phys. Rev. B **77**, 224507 (2008).
[9] R. Castillo, W. Schnelle, M. Bobnar, U. Burkhardt, B. Böhme, M. Baitinger, U. Schwarz, and Y. Grin, Z. Anorg. Allg. Chem. **641**, 206 (2015).
[10] M. Beekman and G. S. Nolas, Int. J. Appl. Ceram. Technol. **4**, 332 (2007).
[11] H. G. von Schnering, Nova acta Leopoldina **59**, 165 (1985).
[12] H. G. von Schnering, Boletin de la Sociedad Chilena de Quimica **33**, 41 (1988).
[13] D. Connetable, Phys. Rev. B **82**, 075209 (2010).
[14] W. Carrillo-Cabrera, S. Budnyk, Y. Prots, and Y. Grin, Z. Anorg. Allg. Chem. **630**, 2267 (2004).
[15] U. Aydemir, C. Candolfi, H. Borrmann, M. Baitinger, A. Ormeci, W. Carrillo-Cabrera, C. Chubilleau, B. Lenoir, A. Dauscher, N. Oeschler, F. Steglich, and Y. Grin, Dalton Trans. **39**, 1078 (2010).
[16] P. Hohenberg and W. Kohn, Phys. Rev. **136**, B864 (1964).
[17] W. Kohn and L. J. Sham, Phys. Rev. **140**, A1133 (1965).
[18] V. Blum, R. Gehrke, F. Hanke, P. Havu, V. Havu, X. Ren, K. Reuter, and M. Scheffler, Comput. Phys. Commun. **180**, 2175 (2009).
[19] F. Knuth, C. Carbogno, V. Atalla, V. Blum, and M. Scheffler, Comput. Phys. Commun. **190**, 33 (2015).
[20] See Supplemental Material [20] at http://link.aps.org/supplemental/10.1103/PhysRevLett.118.236401 for a detailed discussion of the employed methodology (incl. the numerical settings), for the validation of the employed exchange-correlation functional, and for an extended discussion of the vacancy's properties in filled clathrates.
[21] C. W. Weinert and M. Scheffler, Phys. Rev. Lett. **58**, 1456 (1987).
[22] C. Freysoldt, B. Grabowski, T. Hickel, J. Neugebauer, G. Kresse, A. Janotti, and C. G. Van de Walle, Rev. Mod. Phys. **86**, 253 (2014).
[23] J. P. Perdew and Y. Wang, Phys. Rev. B **45**, 13244 (1992).
[24] J. P. Perdew, K. Burke, and M. Ernzerhof, Phys. Rev. Lett. **77**, 3865 (1996).
[25] J. P. Perdew, A. Ruzsinszky, G. I. Csonka, O. A. Vydrov, G. E. Scuseria, L. A. Constantin, X. Zhou, and K. Burke, Phys. Rev. Lett. **100**, 136406 (2008).
[26] B. Hammer, L. B. Hansen, and J. K. Nørskov, Phys. Rev. B **59**, 7413 (1999).
[27] A. V. Krukau, O. A. Vydrov, A. F. Izmaylov, and G. E. Scuseria, J. Chem. Phys. **125**, 224106 (2006).
[28] H. G. von Schnering, M. Schwarz, J.-H. Chang, P. K., E.-M. Peters, and R. Nesper, Z. Kristallogr. New Cryst. Struct. **220**, 525 (2005).
[29] T. Goebel, Y. Prots, and F. Haarmann, Z. Kristallogr. New Cryst. Struct. **224**, 7 (2009).
[30] H. G. von Schnering, J. Llanos, J.-H. Chang, K. Peters, E.-M. Peters, and R. Nesper, Z. Kristallogr. New Cryst. Struct. **220**, 324 (2005).
[31] W. Carrillo-Cabrera, J. Curda, H. G. von Schnering, S. Paschen, and Y. Grin, Z. Kristallogr. New Cryst. Struct. **215**, 207 (2000).
[32] In all cases, the first two vacancies are most favorable at $6c$, the third and fourth at $24k$ positions. However, taking into account superstructure formation in $Ba_8Ge_{43}\square_3$ [15], the experimentally reported vacancy configuration ($2\times2\times2$ superstructure; space group $Ia\bar{3}d$) is found to be slightly more stable by 0.05 (PBEsol) and 0.07 (HSE06) eV/f.u..
[33] J. Llanos, Ph.D. thesis, Stuttgart University, 1984.
[34] U is calculated from Eq. (1), using the expression $U = E^{q+2}_{\square}(\mu_e = 0) + E^{q}_{\square}(\mu_e = 0) - 2E^{q+1}_{\square}(\mu_e = 0)$.
[35] G. A. Baraff, E. O. Kane, and M. Schlüter, Phys. Rev. B **21**, 5662 (1980).
[36] A. Fazzio, A. Janotti, A. J. R. da Silva, and R. Mota, Phys. Rev. B **61**, R2401 (2000).
[37] G. Li, Q. An, W. Li, I. William A. Goddard, P. Zhai, Q. Zhang, and G. J. Snyder, Chem. Mater. **27**, 6329 (2015).
[38] L. Offernes, P. Ravindran, and A. Kjekshus, J. Alloys Compd. **439**, 37 (2007).
[39] M. M. Balakrishnarajan, P. D. Pancharatna, and R. Hoffmann, New J. Chem. **31**, 473 (2007).
[40] M. Johnsson and P. Lemmens, in *Handbook of Magnetism and Advanced Magnetic Materials* (John Wiley and Sons Ltd, Hoboken, New Jersey, 2007).
[41] G. P. Meisner, D. T. Morelli, S. Hu, J. Yang, and C. Uher, Phys. Rev. Lett. **80**, 3551 (1998).
[42] I. Galanakis, E. Şaşıoğlu, S. Blügel, and K. Özdoğan, Phys. Rev. B **90**, 064408 (2014).
[43] R. Schmechel and H. Werheit, J. Phys. Condens. Matter **11**, 6803 (1999).
[44] R.-A. Eichel, Phys. Chem. Chem. Phys. **13**, 368 (2011).
[45] See DOI: 10.17172/NOMAD/2017.05.30-1.